nature cell biology

External push and internal pull forces recruit curvature-sensing N-BAR domain proteins to the plasma membrane

Milos Galic[1,7], Sangmoo Jeong[2], Feng-Chiao Tsai[1], Lydia-Marie Joubert[3], Yi I. Wu[4,6], Klaus M. Hahn[4], Yi Cui[5] and Tobias Meyer[1,7]

Many of the more than 20 mammalian proteins with N-BAR domains[1,2] control cell architecture[3] and endocytosis[4,5] by associating with curved sections of the plasma membrane[6]. It is not well understood whether N-BAR proteins are recruited directly by processes that mechanically curve the plasma membrane or indirectly by plasma-membrane-associated adaptor proteins that recruit proteins with N-BAR domains that then induce membrane curvature. Here, we show that externally induced inward deformation of the plasma membrane by cone-shaped nanostructures (nanocones) and internally induced inward deformation by contracting actin cables both trigger recruitment of isolated N-BAR domains to the curved plasma membrane. Markedly, live-cell imaging in adherent cells showed selective recruitment of full-length N-BAR proteins and isolated N-BAR domains to plasma membrane sub-regions above nanocone stripes. Electron microscopy confirmed that N-BAR domains are recruited to local membrane sites curved by nanocones. We further showed that N-BAR domains are periodically recruited to curved plasma membrane sites during local lamellipodia retraction in the front of migrating cells. Recruitment required myosin-II-generated force applied to plasma-membrane-connected actin cables. Together, our results show that N-BAR domains can be directly recruited to the plasma membrane by external push or internal pull forces that locally curve the plasma membrane.

N-BAR domains are versatile membrane-binding regulatory elements that function in a wide range of cellular processes including regulation of cortical actin structures[3] and clathrin-mediated endocytosis[4,5]. Although the cellular functions of many N-BAR domain proteins have been extensively studied, the fundamental chicken and egg causality dilemma of whether they primarily sense or form curvature is not resolved. This question applies to all curvature binding domains but is particularly relevant for N-BAR domain proteins where *in vitro* assays showed that they selectively bind to[6] as well as form[7] membranes of high positive curvature. During endocytosis, where N-BAR domains have been most extensively studied, the N-BAR domain proteins amphiphysin 1, endophilin 2 and BIN2 are recruited only after the assembly of clathrin-coated pits in a step that preceded vesicle scission[8]. This raised the question of whether N-BAR domain proteins are recruited directly by curved membranes created by clathrin-mediated formation of a tubular neck or indirectly by first binding to adaptor proteins that then recruit N-BAR domains to curve the membrane. Similarly, it is not clear how N-BAR domain proteins that bind[9,10] N-WASP and other actin-binding proteins[11,12] are recruited to actin-rich regions of the plasma membrane to then in turn regulate the actin architecture.

Our study aimed to distinguish between sensing and forming curved membranes by investigating recruitment of N-BAR domain protein to the plasma membrane in living cells. We focused on two examples of N-BAR domains, the one from nadrin 2 (refs 3,13), a regulator of actin polymerization, and the one from amphiphysin 1 (ref. 4), a regulator of endocytosis. We developed a method to directly deform the plasma membrane in live cells using cone-shaped tin oxide nanostructures[14] (nanocones). The top panels in Fig. 1a show top and side electron microscopy (SEM) views of the formed nanocones and the bottom left panel shows a cell growing on top of the nanocone surface.

[1]Department of Chemical and Systems Biology, Stanford University, 318 Campus Drive, Clark Building W200, Stanford, California 94305, USA. [2]Department of Electrical Engineering, Stanford University, 476 Lomita Mall, McCullough Building 217, Stanford, California 94305, USA. [3]Cell Sciences Imaging Facility, Stanford University School of Medicine, Stanford, California 94305, USA. [4]Department of Pharmacology, Lineberger Comprehensive Cancer Center, University of North Carolina, 120 Mason Farm Road, Genetic Medicine Building, Chapel Hill, North Carolina 27599, USA. [5]Department of Materials Science and Engineering, Stanford University, 476 Lomita Mall, McCullough Building 343, Stanford, California 94305, USA. [6]Present address: Center for Cell Analysis and Modeling, University of Conneticut Health Center, 400 Farmington Avenue, Cell and Genome Sciences Building, Farmington, Connecticut 06032, USA.
[7]Correspondence should be addressed to M.G. or T.M. (e-mail: milos@stanford.edu or tobias1@stanford.edu)

Received 1 September 2011; accepted 30 May 2012; published online 1 July 2012; DOI: 10.1038/ncb2533

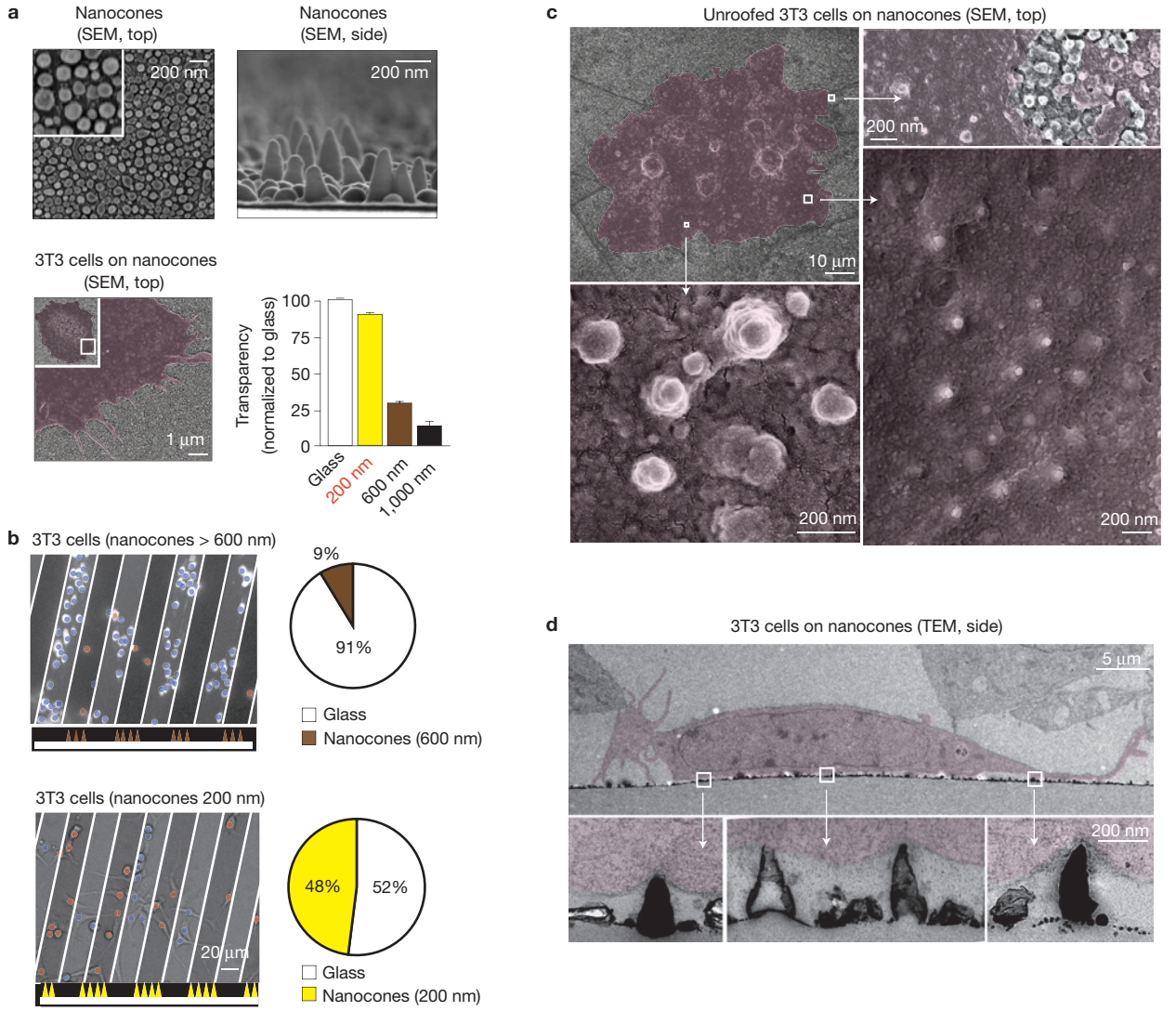

Figure 1 Nanocones induce inward curved plasma membrane deformations at the basal plasma membrane of adherent cells. (**a**) SEM micrographs of nanocones on a glass substrate shown from the top (top, left) and the side (top, right). SEM micrograph of 3T3 cells (red) grown on 200 nm nanocones (bottom, left). Transparency of nanocones decreases with increasing cone height (bottom, right). For each height, the transparency was measured at eight different regions of the sample. Error bars represent s.e.m. of the mean value. (**b**) 3T3 cells cultured on 20-µm-wide stripes of 600 nm nanocones (top, left) and 200 nm nanocones (bottom, left). The sawtooth symbols at the bottom of the panels and the white lines depict the location of the nanocone stripes. Cells on top of nanocones are marked with red, and cells on glass with blue. After 48 h, the cell density on 600 nm cones (brown) is significantly lower when compared with adjacent glass surface, whereas no changes are visible for 200 nm nanocones (yellow). Analyses of cell density for nanocones of 600 nm ($n = 1,484$ cells, top) and 200 nm ($n = 780$ cells, bottom) height are shown to the right. (**c**) SEM micrographs of the inner side of the plasma membrane of cells grown on 200 nm nanocones. Cells were sonicated to remove everything except the plasma membrane of cells grown on nanocones (red). Note the nanocone-induced deformation of the plasma membrane. (**d**) TEM micrographs of 3T3 cells grown on 200 nm nanocones. Cells are coloured in red. Note that nanocones do not penetrate the plasma membrane.

We tested an array of cone sizes that can be formed by this process and found an optimal height of 200 nm with a diameter of 50 nm at the base. The 200 nm nanocones had a 90% transparency compared with glass without nanocones (Fig. 1a, bottom right). When cultured on 200 nm but not on 600 nm nanocones, cells showed no significant preference between nanocone and flat surfaces (Fig. 1b) and freely migrated across 20-µm-wide bands of nanocones (data not shown). When culturing cells on these nanocones, we found small-diameter positively curved sections (inward bend) in the basal plasma membrane of unroofed cells in SEM micrographs (Fig. 1c), and in transmission electron microscopy (TEM) images of cross-sections of the basal plasma membrane (Fig. 1d).

To compare the effect of nanocone-induced plasma membrane curvatures on N-BAR domain recruitment within the same cell, we designed a pattern of 3-µm-wide stripes, alternating between smooth and nanocone-coated surfaces, plated 3T3 cells expressing fluorescently tagged N-BAR proteins on these patterned nanostructures and imaged them with a confocal microscope. Markedly, we found puncta selectively over nanocone stripes when we expressed the YFP-conjugated N-BAR protein nadrin 2 (Fig. 2a). Control experiments

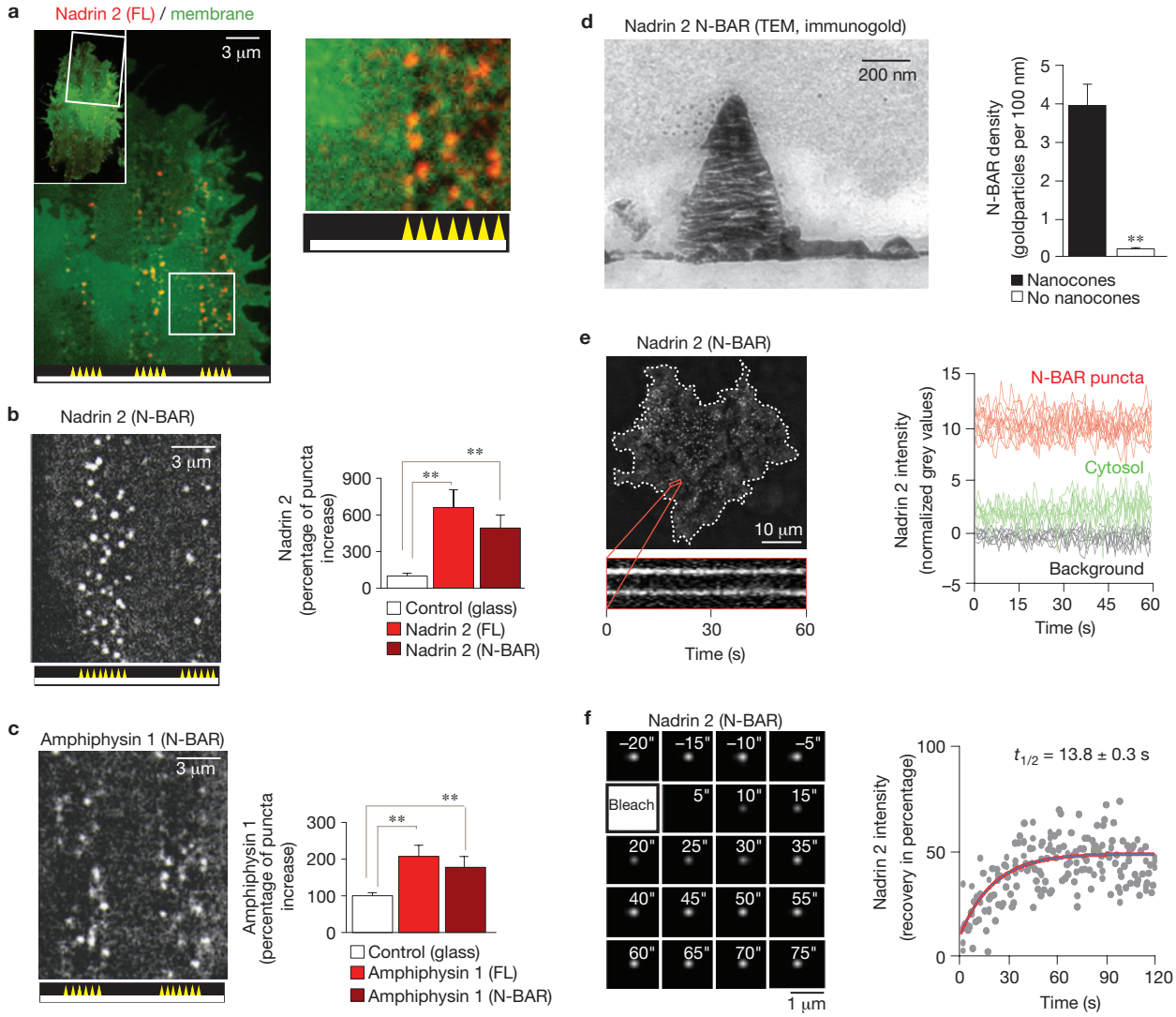

Figure 2 Nanocone-induced membrane deformation triggers N-BAR domain recruitment to the plasma membrane. (**a**) Nadrin 2 forms puncta over nanocones. 3T3 cells were grown on 3-μm-wide stripes of nanocones and transfected with nadrin 2 (red) together with membrane marker CAAX (green). Nadrin 2 puncta formation was selectively observed over nanocone stripes. A magnification of a selected region (white rectangle) is shown to the right. (**b**,**c**) The N-BAR domain is sufficient for puncta formation. Quantitative analysis of the increase in puncta density induced by nanocones for full-length (FL, light red, $n = 14$ cells) and the isolated N-BAR domain (N-BAR, dark red, $n = 12$ cells) of nadrin 2 (**b**) and full-length (light red, $n = 10$ cells) and the isolated N-BAR domain (dark red, $n = 12$ cells) of amphiphysin 1 (**c**), respectively. Error bars represent s.e.m. of the mean value. (**d**) TEM micrograph showing that the N-BAR domain of nadrin 2 accumulates on membrane deformations induced by nanocones. 3T3 cells were transfected with the fluorescently tagged N-BAR domain of nadrin 2, fixed and incubated with primary antibodies directed against the fluorescent tag. Note that gold-conjugated secondary antibodies accumulate over nanocone-induced inward membrane deformations. The immunogold density was measured over nanocones ($n = 25$) where deformation of the plasma membrane was observed and compared with adjacent regions within the same image. Error bars represent s.e.m. of the mean value. (**e**) Nanocone-induced N-BAR domain puncta of nadrin 2 are stationary and long-lived. 3T3 cells plated on nanocones were transfected with the fluorescently tagged N-BAR domain of nadrin 2 and imaged every 500 ms for 60 s. Kymograph of two representative puncta (orange) is shown below. To the right, a graph depicting traces of individual N-BAR domain puncta (red), cytosol (green) and background (black) is shown. (**f**) FRAP analysis indicates a stable, long-lasting and dynamic fraction of comparable sizes over individual nanocones. Magnified area showing a time-series following a single nanocone-induced N-BAR domain accumulation through a FRAP cycle (left) and analysis of multiple experiments (right) are shown. About half of the BAR domains present in the puncta are exchanged with a half-life ($t_{1/2}$) of ~14 s.

showed that the average local increase in nadrin 2 intensity in puncta was 113 ± 9% over a uniform cytosolic background whereas a plasma membrane marker increased at the same sites only by 45 ± 3%, arguing that nadrin 2 is recruited to local sites within the plasma membrane. A correlation analysis resulted in the same conclusion (Supplementary Fig. S1a,b).

We then showed that the N-BAR domain of nadrin 2 is sufficient to mediate the punctuate recruitment to the regions with nanocone stripes (Fig. 2b left). In a quantitative single-cell analysis, full-length protein and the isolated N-BAR domain generated significantly more puncta in the plasma membrane over nanocone stripes when compared with the plasma membrane over the flat surfaces (Fig. 2b, right panel).

This recruitment by nanocone stripes was not restricted to the N-BAR domain of nadrin 2, but also applied to the isolated N-BAR domain of amphiphysin 1 (Fig. 2c).

Using electron micrographs, we then validated the precise localization of the N-BAR domain over nanocones. Staining cells transfected with the YFP-tagged N-BAR domain of nadrin 2 with an antibody directed against the fluorescent tag showed a significant enrichment of gold particles over nanocones (Fig. 2d and Supplementary Fig. S1c). Next, we measured the persistence of N-BAR domain puncta over nanocones in live cells. We found the puncta themselves to be stable for periods longer than 1 min (Fig. 2e), whereas about half of the BAR domains within the puncta exchanged with a time constant of ~14 s, as shown in fluorescence recovery after photobleaching (FRAP) experiments (Fig. 2f).

As many N-BAR domain proteins have roles in endocytosis[4,5], we determined, as a control, whether the observed puncta reflect endocytotic sites that might be induced by nanocones. We did not observe a nanocone-dependent increase in the average endocytosis rate (Supplementary Fig. S2a). Although, clathrin light chain and dynamin both enriched over stripes of nanocones (Supplementary Fig. S2b,c), co-expression experiments with nadrin 2 and clathrin light chain showed only minimal overlap (Supplementary Fig. S2d), arguing that N-BAR domain recruitment by nanocones can be induced independently of endocytosis. This low correlation was confirmed in a spatial cross-correlation analysis where the co-localization of the near identical CFP-tagged nadrin 2 and YFP-tagged nadrin 2 was used as a reference (Supplementary Fig. S2e,f). Tracking individual CFP–clathrin light chain puncta over nanocones over time provided no evidence for sequential co-localization, ruling out that N-BAR domain recruitment follows clathrin accumulation with a delay (Supplementary Fig. S2g). Together, these results argue that nanocones provide an external local push force that induces stable membrane deformations and that an inward curved plasma membrane is sufficient to recruit N-BAR domains.

We then considered that internal forces that pull on local membrane sites during actin reorganization or endocytosis might be equally capable of inducing the high inward curvatures necessary for N-BAR domain recruitment. We tested this hypothesis by focusing on migrating cells that experience significant membrane deformation at the leading edge[15]. As shown in Fig. 3a, the plasma membrane-localized N-BAR domain proteins nadrin 2 and amphiphysin 1 were enriched in the actin-rich front of polarized migrating 3T3 cells. This localization only required the N-BAR domain, because the same polarized localization was observed for full-length and isolated N-BAR domains of nadrin 2 and amphiphysin 1 (Fig. 3b). Deletion of the amphipatic helix, a sequence motif required for binding and stabilization of curved membranes[7,16,17], prevented enrichment of the N-BAR domain protein, arguing that localization critically depends on this structural feature required for membrane binding and present in all N-BAR domain proteins (Fig. 3c).

We observed an overlap between membrane regions with high cortical actin and either nadrin 2 or amphiphysin 1 N-BAR domains, suggesting that curved membrane sites are created above cortical actin networks (Fig. 3d). Control experiments with markers for the cytoplasm and the plasma membrane showed that this partial co-localization of N-BAR domains with cortical actin was not caused by variability in cell thickness or membrane accumulation (Fig. 3a,b,e). Furthermore, the N-BAR domain of nadrin 2 did not co-localize with a marker for clathrin-mediated endocytosis at the leading edge (Supplementary Fig. S2h). However, we observed transient co-localization with clathrin puncta behind the leading edge, suggestive of temporary recruitment of the isolated N-BAR domain of nadrin 2 to these internal sites during endocytosis[8,18] (Supplementary Fig. S2i). Together, these results argued that N-BAR domain proteins are recruited to the actin-rich leading-edge membrane in a process that does not involve endocytosis and can be mediated by their N-BAR domains alone.

To more directly investigate the effect of peripheral actin polymerization on the localization of N-BAR domains in the front, we transiently changed actin dynamics in live cells. First, we monitored N-BAR domain puncta at the leading edge of 3T3 cells on depolymerization of actin filaments. N-BAR domain puncta disappeared within less than 5 min after the addition of 4 μM latrunculin A (Fig. 3f) or 5 μM cytochalasin D (Fig. 3g) and reappeared once the drug was washed out. In a complementary experiment, we rapidly triggered actin polymerization taking advantage of an assay based on inducible translocation of TIAM1, an exchange factor for RAC (ref. 19). 3T3 cells were co-transfected with a fluorescently tagged N-BAR domain together with a construct containing FKBP fused to TIAM1 and a membrane-anchored FRB domain. The addition of rapamycin triggered dimerization of FRB and FKBP, rapidly recruiting TIAM1 to the plasma membrane, and causing the activation of the small GTPase RAC1. This led to increased levels of RAC–GTP at the plasma membrane causing extensive actin polymerizations and, with a delay, the translocation of the isolated N-BAR domain to the plasma membrane (Supplementary Fig. S3). A comparable result was observed when a photoactivatable version of the small GTPase RAC1 (LOV–RAC1; ref. 20) was used to trigger actin polymerization (Supplementary Fig. S4). Together, these experiments argue that increases in dynamic cortical actin polymerization result, with a delay, in the recruitment of curvature-sensing N-BAR domain proteins.

Cortical actin polymerization often occurs in cycles where a polymerization phase that extends the lamellipodia outward is followed by a retraction phase whereby the actin motor myosin II pulls lamellipodia partially back before the next extension[21–23]. Markedly, time-lapse imaging of cyclic lamellipodia in the front of polarized 3T3 cells showed that N-BAR recruitment occurs primarily during the retraction phase rather than the extension/polymerization phase (Fig. 4a). A time-course analysis over multiple expansion–retraction cycles showed that the concentration of the N-BAR domain (normalized to the total amount of actin filaments) remained low as the lamellipodia moved outward and only increased as it was retracted (Fig. 4b and Supplementary Movie S1). This observation was confirmed using an autocorrelation analysis comparing normalized N-BAR domain concentration and lamellipodia position (Fig. 4c). This cyclic nature of N-BAR domain recruitment during extension and retraction is schematically shown in Fig. 4d.

We reasoned that myosin-II-mediated lamellipodia retraction involves pulling forces applied to the plasma membrane through membrane-anchored actin cables that cause local inward membrane curvature while the distributed surrounding actin meshwork resists the retraction. Consistent with such a role of myosin II, we observed

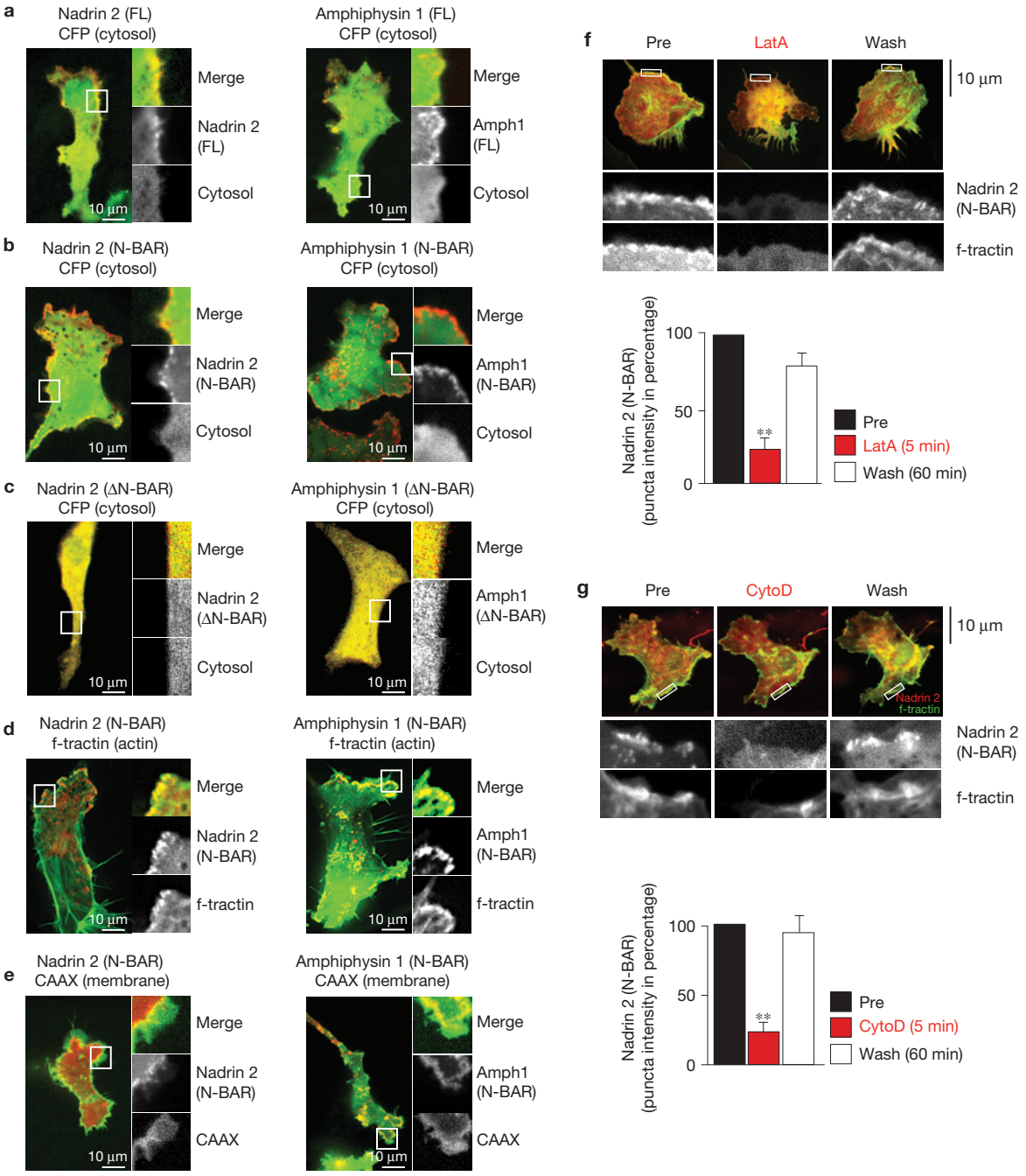

Figure 3 N-BAR domains are dynamically recruited to local membrane sites at the leading edge of migrating 3T3 cells. (**a**) The proteins nadrin 2 and amphiphysin 1 are enriched in the leading edge of migrating 3T3 cells. (**b**) Enrichment in the leading edge is dependent on the N-BAR domain. Cells expressing a cytosolic marker (CFP, green) and the isolated N-BAR domain of nadrin 2 (left, red) and amphiphysin 1 (right, red). Note the polarized localization of the isolated N-BAR domain to the leading edge. (**c**) Enrichment in the leading edge is dependent on the amphipatic helix. Cells expressing a cytosolic marker (CFP, green) and the isolated N-BAR domain of nadrin 2 (left, red) and amphiphysin 1 (right, red) that is lacking the amino-terminal amphipatic helix show no polarized localization to the leading edge. (**d**) N-BAR domain patches show significant overlap with marker for filamentous actin (f-tractin). 3T3 cells were transfected with a marker for filamentous actin (green) and the N-BAR domain of nadrin 2 (left, red) or amphiphysin 1 (right, red), respectively. (**e**) N-BAR domain and a plasma membrane marker only partially overlap. 3T3 cells transfected with a membrane marker (CAAX, green) and the N-BAR domain of nadrin 2 (left, red) and amphiphysin 1 (right, red) are shown. (**f**) The addition of the actin polymerization inhibitor latrunculin A (LatA) reversibly inhibits N-BAR domain puncta formation. A total of 1,303 individual puncta from 12 cells were analysed for the drug washout experiments. Pre, pre-treatment. (**g**) Addition of the actin polymerization inhibitor cytochalasin D (CytoD) reversibly inhibits N-BAR domain puncta formation. A total of 428 puncta from eight cells were analysed for the drug washout experiments. Error bars represent s.e.m. of the mean value. $^{**}P < 0.01$.

during lamellipodia retraction a parallel increase of the N-BAR domain of nadrin 2 at the front and of the heavy chain of non-muscle myosin II-A (NMHC-II-A) in a region closely behind where the lamellipodia transitions into the lamella (Fig. 4e and Supplementary Movie S2). To further validate the hypothesis that myosin II may pull on actin cables to promote retraction, we used ML-7, an inhibitor of myosin light

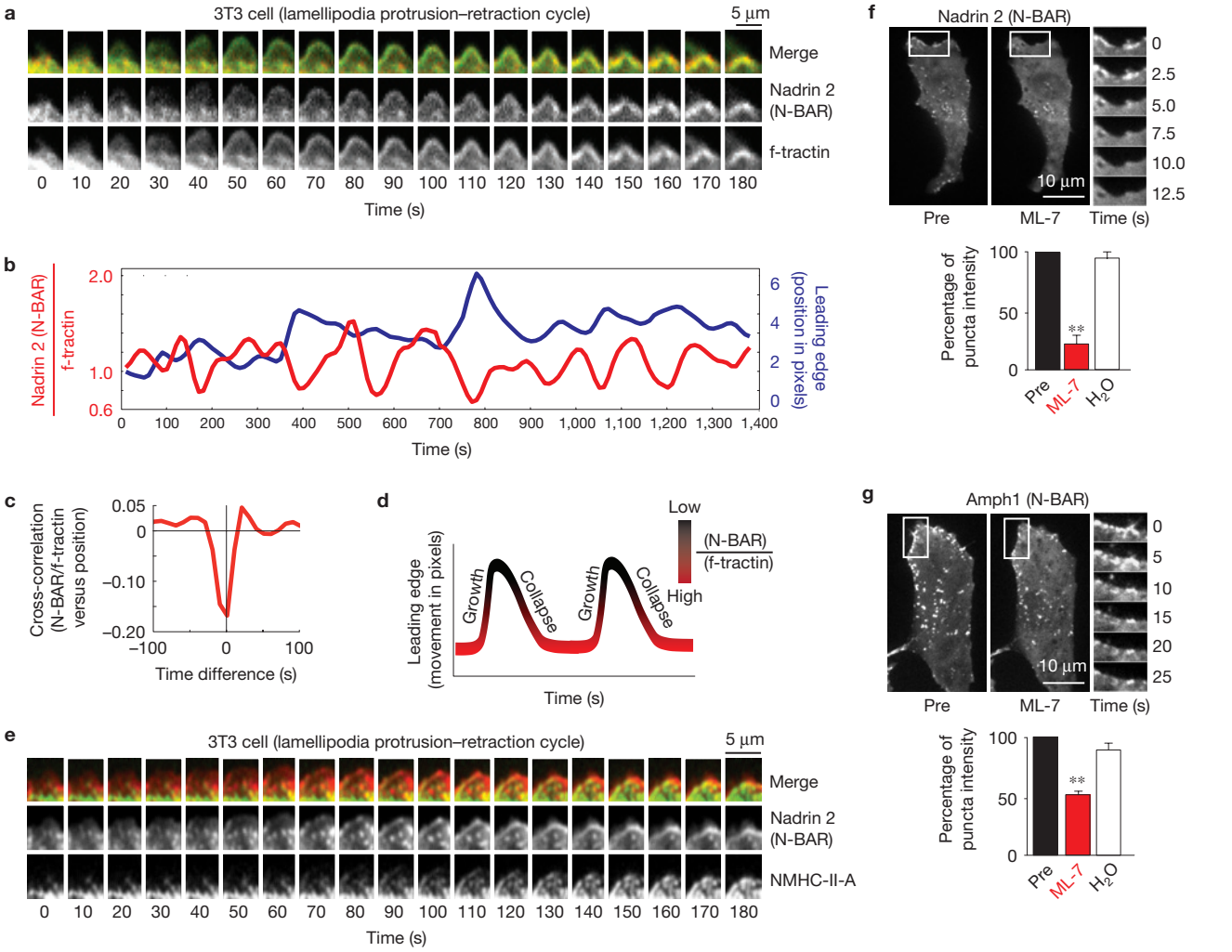

Figure 4 Myosin-II-dependent contraction of actin cables induces N-BAR domain recruitment to the lamellipodia plasma membrane. (**a**) N-BAR domain of nadrin 2 recruits to contracting lamellipodia. Montage depicting an expansion–collapse cycle in 3T3 cell lamellipodia. Merged images of the N-BAR domain of nadrin 2 (red) and f-tractin (green) at an interval of 10 s are shown in the top row. For clarification, separate channels of the fluorescently tagged N-BAR domain of nadrin 2 (middle row) and f-tractin (bottom row) are shown below. Note the delayed accumulation of nadrin 2 during the retractive phase of lamellipodia. (**b**) Comparison of normalized N-BAR domain intensity during an expansion–collapse cycle of the lamellipodia. Correlation of the N-BAR domain concentration normalized to f-tractin (red) and lamellipodia position (blue) are shown for an individual position on the leading edge monitored over an interval of 1,400 s. (**c**) The fluorescence level of the N-BAR domain (after normalization to f-tractin intensity) anti-correlates with the expansion of the leading edge. Graph depicting the average cross-correlation of the normalized N-BAR concentration at the leading edge with the position of the leading edge over time. (**d**) Model of the normalized N-BAR domain of nadrin 2 concentration as a function of the leading-edge position. (**e**) NMHC-II-A and the N-BAR domain of nadrin 2 both enrich during lamellipodia retraction, N-BAR close to the front and myosin II a bit further back. The montage of a 3T3 cell expressing nadrin 2 (red) and NMHC-II-A (green) shows accumulation of both proteins during lamella retraction. (**f**,**g**) Inhibition of myosin II causes rapid disassembly of N-BAR domain puncta at the leading edge of 3T3 cells. The addition of the MLCK inhibitor ML-7 triggers rapid disassembly of the N-BAR domain of nadrin 2 (**f**, red, $n = 8$ cells) and amphiphysin 1 (**g**, red, $n = 12$ cells) puncta, respectively. In contrast, no effect was visible on the addition of water (white, $n = 6$ cells). For better visualization, a montage of a magnified section is depicted next to the pictures. Error bars represent s.e.m. of the mean value, $^{**}P < 0.01$.

chain kinase (MLCK) that controls myosin II activity of non-muscle cells. Consistent with a key role for MLCK and myosin II in the process of N-BAR domain recruitment, the patches of the respective N-BAR domains of nadrin 2 and amphiphysin 1 rapidly disappeared on the addition of the inhibitor (Fig. 4f,g).

This suggested that myosin-II-mediated force on actin cables induces local inward deformations of the plasma membrane at sites where the cables contact the leading-edge plasma membrane. We used electron microscopy[24] to analyse the topography of the plasma membrane of migrating cells and observed significant inward curved sections along the leading edge (Fig. 5a). Actin cables oriented perpendicular to the plasma membrane often pointed to the inward curved section of the plasma membrane (Fig. 5b and Supplementary Fig. S5a), suggesting that force applied to these actin cables was responsible for the deformation. Furthermore, immunogold localization showed that the isolated N-BAR domain of nadrin 2 locally enriched at these inward curved membrane sites (Fig. 5c and Supplementary Fig. S5b). Together, these findings introduce a recruitment mechanism whereby

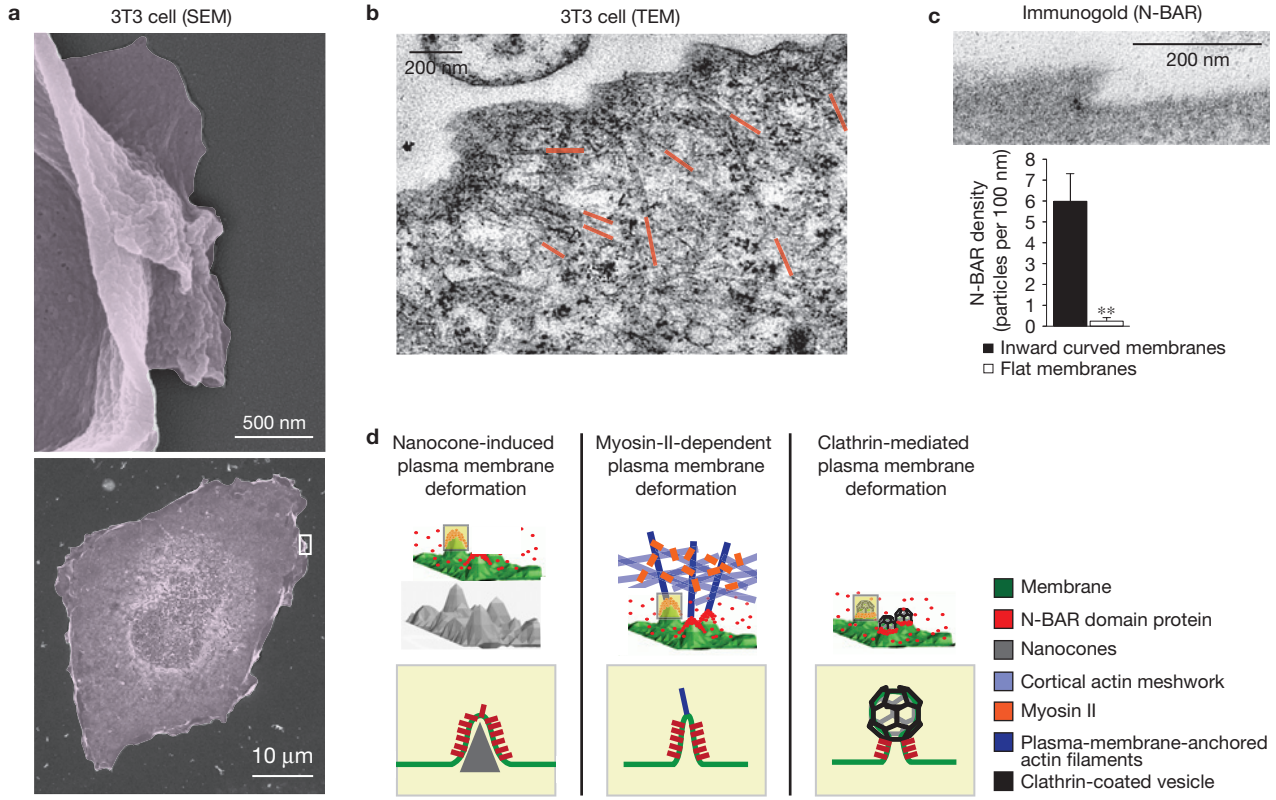

Figure 5 External push and internal pull forces applied to local plasma membrane sites recruit N-BAR domains to inward curved membrane. (**a**) SEM micrographs depicting membrane deformation at the leading edge. For better visualization, a magnification of a selected region (white rectangle, bottom) depicting a lamellipodium is shown (top). (**b**) TEM micrograph of a 3T3 cell parallel to the glass plane indicating actin filaments pulling at the plasma membrane as a source of plasma deformation. For better visualization the ends of individual actin cables are highlighted in red. (**c**) The N-BAR domain of nadrin 2 accumulates on membrane deformations at the leading edge. 3T3 cells were transfected with the fluorescently tagged N-BAR domain of nadrin 2, fixed and incubated with primary antibodies directed against the fluorescent tag. Enrichment of immunogold particles to curved sites was measured ($n = 15$ cells) and compared to adjacent regions within the same image. Note that gold-conjugated secondary antibody is significantly enriched on inward curved membrane sites (graph, bottom). (**d**) Different types of force-dependent membrane deformation recruit N-BAR domain proteins. N-BAR domain proteins (red) sense positive (inward) membrane curvature induced by external force such as the nanocone substrate (left), during myosin-II-triggered actin contraction (middle), and during endocytosis (right). Error bars represent s.e.m. of the mean value; $^{**}P < 0.01$.

MLCK and myosin-II-mediated actin contraction pulls on local plasma membrane–actin cable contact sites to create local inward curved membrane sites that then recruit N-BAR domain proteins. Notably, N-BAR puncta disappeared when plasma membrane tension was increased by lowering the external osmotic strength (Supplementary Fig. S5c). Correspondingly, lowering the membrane tension with high osmotic pressure or the surface relaxant deoxycholate[25] triggered puncta formation (Supplementary Fig. S5d,e), suggesting that N-BAR recruitment can further be regulated by changes in the global plasma membrane tension parameter.

Our results argue that different modes of mechanical deformation of the plasma membrane exist that trigger the recruitment of N-BAR-domain-containing regulatory proteins. First, the ability of external nanocones to directly trigger N-BAR domain recruitment suggests that a receptor-independent mechanical signalling mechanism may exist whereby extracellular matrix components of sufficient stiffness can trigger local deformations of the plasma membrane to directly recruit and activate intracellular signalling proteins with N-BAR domains (Fig. 5d, left). Second, our results with actin and myosin II argued that internal force applied to membrane connected actin cables can exert sufficient pull force to curve the plasma membrane and cause N-BAR domain recruitment (Fig. 5d, middle), a finding that has broad implications in actin-dependent processes such as cell polarization and migration. Third, our results also probably apply to endocytosis where clathrin coats may provide the force that recruits N-BAR domains by creating a neck with a curved membrane tube that connects the forming clathrin vesicle to the rest of the plasma membrane (ref. 8; Fig. 5d, right). Although these different recruitment mechanisms argue that local force application and induction of membrane curvature are needed to trigger the initial N-BAR domain recruitment in live cells, it is likely that N-BAR domains, once recruited, have a complementary role in stabilizing the curved membrane section.

Our study shows that cytosolic N-BAR domains continuously scan the plasma membrane for highly inward curved sections and accumulate at sites where the membrane is sufficiently deformed by local forces. Our study further suggests that any type of push force applied to local plasma membrane sites from the outside or pull force applied to local sites from the inside will induce N-BAR domain recruitment as long as the local force is sufficiently strong and is counteracted by distributed forces on the membrane in the opposing direction. Finally, different force-generating mechanisms involving clathrin, microtubules, actin cables or extracellular matrix

may create in different contexts either inward (positive) or outward (negative) curved plasma membrane that probably provides only two types of distinct recruitment signal. To gain specificity, additional co-regulatory mechanisms are probably needed to link specific mechanical deformations to distinct signalling pathways and cell functions. □

METHODS

Methods and any associated references are available in the online version of the paper at www.nature.com/naturecellbiology

Note: Supplementary Information is available on the Nature Cell Biology website

ACKNOWLEDGEMENTS

The authors thank the members of the Meyer laboratory for comments and discussion. M.G. was supported by the Swiss National Science Foundation (No. PBBSP3-123159), and a Novartis Jubilaeumsstiftung and Stanford Deans Postdoctoral Fellowship. S.J. was supported by a Korea Foundation for Advanced Studies graduate fellowship. Y.C. acknowledges the partial support from a DOE-EFRC at Stanford: Center on Nanostructuring for Efficient Energy Conversion (No. DE-SC0001060). T.M. acknowledges financial support from the National Institutes of Health, MH064801, MH095087 and GM063702.

AUTHOR CONTRIBUTIONS

M.G. performed all experiments and analysed the data. F-C.T. developed the temporal cross-correlation analysis. S.J. and Y.C. designed the nanocones. L-M.J. helped with the SEM. Y.I.W. and K.M.H. developed the photoactivatable RAC construct. M.G. and T.M. designed the experiments, interpreted the results and wrote the manuscript. All authors discussed the results and the manuscript. T.M. supervised the study.

COMPETING FINANCIAL INTERESTS

The authors declare no competing financial interests.

Published online at www.nature.com/naturecellbiology
Reprints and permissions information is available online at www.nature.com/reprints

1. Habermann, B. The BAR-domain family of proteins: a case of bending and binding? *EMBO Rep.* **5,** 250–255 (2004).
2. Suetsugu, S., Toyooka, K. & Senju, Y. Subcellular membrane curvature mediated by the BAR domain superfamily proteins. *Semin. Cell Dev. Biol.* **21,** 340–349 (2010).
3. Rollason, R., Korolchuk, V., Hamilton, C., Jepson, M. & Banting, G. A CD317/tetherin-RICH2 complex plays a critical role in the organization of the subapical actin cytoskeleton in polarized epithelial cells. *J. Cell Biol.* **184,** 721–736 (2009).
4. David, C., McPherson, P. S., Mundigl, O. & de Camilli, P. A role of amphiphysin in synaptic vesicle endocytosis suggested by its binding to dynamin in nerve terminals. *Proc. Natl Acad. Sci. USA* **93,** 331–335 (1996).
5. Ringstad, N. *et al.* Endophilin/SH3p4 is required for the transition from early to late stages in clathrin-mediated synaptic vesicle endocytosis. *Neuron* **24,** 143–154 (1999).
6. Bhatia, V. K. *et al.* Amphipathic motifs in BAR domains are essential for membrane curvature sensing. *EMBO J.* **28,** 3303–3314 (2009).
7. Peter, B. J. *et al.* BAR domains as sensors of membrane curvature: the amphiphysin BAR structure. *Science* **303,** 495–499 (2004).
8. Taylor, M. J., Perrais, D. & Merrifield, C. J. A high precision survey of the molecular dynamics of mammalian clathrin-mediated endocytosis. *PLoS Biol.* **9,** e1000604 (2011).
9. Yamada, H. *et al.* Dynamic interaction of amphiphysin with N-WASP regulates actin assembly. *J. Biol. Chem.* **284,** 34244–34256 (2009).
10. Yarar, D., Waterman-Storer, C. M. & Schmid, S. L. SNX9 couples actin assembly to phosphoinositide signals and is required for membrane remodeling during endocytosis. *Dev. Cell* **13,** 43–56 (2007).
11. Rocca, D. L., Martin, S., Jenkins, E. L. & Hanley, J. G. Inhibition of Arp2/3-mediated actin polymerization by PICK1 regulates neuronal morphology and AMPA receptor endocytosis. *Nat. Cell Biol.* **10,** 259–271 (2008).
12. Salazar, M. A. *et al.* Tuba, a novel protein containing bin/amphiphysin/Rvs and Dbl homology domains, links dynamin to regulation of the actin cytoskeleton. *J. Biol. Chem.* **278,** 49031–49043 (2003).
13. Richnau, N. & Aspenstrom, P. Rich, a ρ GTPase-activating protein domain-containing protein involved in signaling by Cdc42 and RAC1. *J. Biol. Chem.* **276,** 35060–35070 (2001).
14. Jeong, S., McDowell, M. T. & Cui, Y. Low-temperature self-catalytic growth of tin oxide nanocones over large areas. *ACS Nano* **5,** 5800–5807 (2011).
15. Giannone, G. *et al.* Periodic lamellipodial contractions correlate with rearward actin waves. *Cell* **116,** 431–443 (2004).
16. Gallop, J. L. *et al.* Mechanism of endophilin N-BAR domain-mediated membrane curvature. *EMBO J.* **25,** 2898–2910 (2006).
17. Masuda, M. *et al.* Endophilin BAR domain drives membrane curvature by two newly identified structure-based mechanisms. *EMBO J.* **25,** 2889–2897 (2006).
18. Ferguson, S. M. *et al.* Coordinated actions of actin and BAR proteins upstream of dynamin at endocytic clathrin-coated pits. *Dev. Cell* **17,** 811–822 (2009).
19. Inoue, T. & Meyer, T. Synthetic activation of endogenous PI3K and Rac identifies an AND-gate switch for cell polarization and migration. *PLoS One* **3,** e3068 (2008).
20. Wu, Y. I. *et al.* A genetically encoded photoactivatable Rac controls the motility of living cells. *Nature* **461,** 104–108 (2009).
21. Burnette, D. T. *et al.* A role for actin arcs in the leading-edge advance of migrating cells. *Nat. Cell Biol.* **13,** 371–381 (2011).
22. Machacek, M. *et al.* Coordination of ρ GTPase activities during cell protrusion. *Nature* **461,** 99–103 (2009).
23. Giannone, G. *et al.* Lamellipodial actin mechanically links myosin activity with adhesion-site formation. *Cell* **128,** 561–575 (2007).
24. Abercrombie, M., Heaysman, J. E. & Pegrum, S. M. The locomotion of fibroblasts in culture. IV. Electron microscopy of the leading lamella. *Exp. Cell Res.* **67,** 359–367 (1971).
25. Raucher, D. & Sheetz, M. P. Cell spreading and lamellipodial extension rate is regulated by membrane tension. *J. Cell Biol.* **148,** 127–136 (2000).

METHODS

Nanocone formation. A thin film of tin (35 nm thickness) was deposited by electron-beam evaporation on a glass coverslip at room temperature. The glass with the deposited tin was then exposed to a nitrogen gas environment with a low concentration of oxygen (about 1 part per million) and heated to 350 °C for 90 min. To make the nanocone structures transparent, the glass coverslip with nanocones was further heated to 400 °C for 3 h in air. The annealing to the glass and the formation of the replicate nanocone shapes occurred during this step.

Electron micrographs. 3T3 cell were cultured on nanocone-coated glass coverslips and fixed using 2% glutaraldehyde (8% stock EM grade) and 4% paraformaldehyde in 0.1 M HEPES, Na cacodylate buffer at pH ~7.4 for 10 min.

For the TEM micrographs in Figs 1d, 5b and Supplementary Fig. S5a, the fixation medium was then replaced with 1% OsO_4 in double-distilled H_2O (ddH_2O) for 1 h, and the cells were washed three times in ddH_2O and incubated with 1% uranyl acetate in ddH_2O overnight. Samples were then dehydrated as follows: 1× 50% ethanol for 5 min; 1× 70% ethanol for 5 min; 1× 95% ethanol for 10 min; 2× 100% ethanol for 15 min; and finally moved to propylene oxide for 15 min. Epon (20 ml EMbed 812, 16 ml DDSA, 8 ml NMA, 0.77 ml DMP-90) was prepared and sample infiltration performed in a series of steps: 1:1 (Epon/propylene oxide) for 1 h; 2:1 (Epon/propylene oxide) overnight; 100% Epon for 3 h; fresh 100% Epon for 2 h. After the final step, the Epon was polymerized at 65 °C overnight. The glass coverslips and nanocones were then dissolved in 49% hydrofluoric acid (10 min), and samples were washed three times with ddH_2O. Samples were then embedded a second time in Epon and polymerized overnight. Finally, samples were cut orthogonally to the plane of the glass slide and imaged on a JEM-1230 electron microscope using ×5 to ×30,000 magnification.

For the SEM micrographs in Figs 1a,c and 5a, cells were rinsed with 0.1 M Na cacodylate buffer (pH 7.2) after primary fixation and were postfixed for 1 h with 1% OsO_4 in water, washed briefly with water and dehydrated in an ascending ethanol series (50, 70, 90 and 100% (twice), 20 min each) before critical-point drying with liquid CO_2 in a Tousimis 815B. Filters were mounted on colloidal graphite on 15 mm aluminium stubs (Ted Pella), and the upper portion of the well was cut away to retain only the filter area with attached cells for SEM visualization. Mounted specimens were sputter-coated with 100 Å Au/Pd using a Denton Desk 11 TSC sputter coater. Visualization of samples was performed with a Zeiss Sihma field-emission SEM operated at 5 kV, working distance 6 mm and an inlens SE detector under high vacuum conditions. Images were captured in TIFF format.

For the SEM micrograph in Fig. 1c, 3T3 cells were unroofed, by brief sonication (Sonics Vibracell, VCX130). In detail, cells were fixed using 2% glutaraldehyde (8% stock EM grade) and 4% paraformaldehyde in 0.1 M HEPES, Na cacodylate buffer at pH ~7.4 for 10 min. The fixation medium was then replaced with 1× PBS and the samples were placed in a 15 ml glass beaker filled with 10 ml of 1× PBS. A 1/8 inch microprobe was placed 1 cm above the sample in the beaker and two 5 s pulses of 40% intensity were applied. Cells were then put back into the fixation solution and processed as described above.

For the TEM micrographs in Figs 2d, 5c and Supplementary Figs S1c and S5b, 3T3 cells were transiently transfected with the fluorescently tagged isolated N-BAR domain of nadrin 2. At 24 h post-transfection, the cells were FACS sorted and the YFP-positive cells were plated and fixed. The N-BAR domain of nadrin 2 was detected using polyclonal antibodies directed against the fluorescent tag (Invitrogen, A11122, 1:500) and visualized using gold-conjugated secondary antibodies (Ted Pella, 15726-1, 1:50).

Cloning. Double-stranded oligonucleotides encoding full-length and BAR domains of the respective proteins were cloned into the pECFP–N3 or pEYFP–N3 expression vectors (CLONTECH Laboratories). All constructs were validated by sequencing before use. The following primers (with selective restriction sites) were used.

For full-length nadrin 2 (Entrez Gene ID: 9912), 5′-AGCCTTCGAATTCATGAAGAAGCAGTTCAATCGCATGC-3′ and 5′-AGCCTTCGGTACCTCCTGCGCCGAGGGCGGTGCTCTCAGACTCCTC-3′were used. The nadrin 2 N-BAR domain is predicted to be encoded by amino acids 1–244 (ref. 7). Our construct contained an additional linker of 10 amino acids. The sequences 5′-AGCCTTCGAATTCATGAAGAAGCAGTTCAATCGCATGC-3′ and 5′-AGCCTTCGGTACCTCCTGCGCCCCCGAAGGAAGGCTTCTCTAC-3′ were used as primers. The ΔN-BAR construct, lacking the initial amphipatic helix, was encoded following previous publications[7,16,17] by amino acids 18–254 using the following primers: 5′-AGCCTTCGAATTCATGGCTGAAAAGACAGAAGTT-3′ and 5′-AGCCTTCGGTACCTCCTGCGCCCCCGAAGGAAGGCTTC-3′.

Full-length amphiphysin 1 (Entrez Gene ID: 273) was obtained from the ORFeome library (internal ID: 8429). The N-BAR domain of amphiphysin 1 spans amino acids 1–236 (ref. 7). A 20-amino-acid additional linker sequence was included. The primers were 5′-CACCATGGCCGACATCAAGACGG-3′ and 5′-GCGGAGAGGACCCGAATCAC-3′. The ΔN-BAR construct, lacking the initial amphipatic helix, was encoded following previous publications[7,16,17] by amino acids 28–256 using the following primers: 5′-AGCCTTCCTCGAGATGCTGGGGAAAGCTGATGAG-3′ and 5′-AGCCTTCGAATTCGCGGAGAGGACCCGAATC-3′.

Full-length nadrin 1 (Entrez Gene ID: 55114) was obtained from the ORFeome library (internal ID: 14668). The N-BAR domain spanning amino acids 1–260 was generated using the following primers: 5′-AGCCTTCGAATTCATGAAGAAGCAGTTCAACCGC-3′ and 5′-AGCCTTCGGTACCCCTCTTCAGGTGTTCTTC-3′. The ΔN-BAR construct, lacking the initial amphipatic helix, was encoded by amino acids 18–260 using the following primers: 5′-AGCCTTCGAATTCATGGCTGAGAAAACAGAAGTC-3′ and 5′-AGCCTTCGGTACCCCTCTTCAGGTGTTCTTC-3′.

Full-length GMIP (Entrez Gene ID: 51291) was obtained from the ORFeome library (internal ID: 54593).

Full-length TRIP10 (Entrez Gene ID: 9322) was obtained from the ORFeome library (internal ID: 6046). The crystal structure of TRIP10 has previously been solved[26]. To generate the isolated F-BAR domain construct, we used the following primers decoding amino acids 1–298: 5′-AGCCTTCAAGCTTATGGATTGGGGCACTGAG-3′ and 5′-AGCCTTCCGGTACCGCTGTCGGAGGGTGCACG-3′.

Full-length FCHO2 (Entrez Gene ID: 115548) was obtained from the ORFeome library (internal ID: 7370). The crystal structure of FCHO2 has previously been solved[27]. To generate the isolated F-BAR domain construct, we used the following primers decoding amino acids 1–274: 5′-AGCCTTCGAATTCATGATGATGGCGTATTTCGTCGAG-3′ and 5′-AGCCTTCGGTACCAGCAGTGTCACATTCTTC-3′.

Full-length BAIAP2 (Entrez Gene ID: 10458) was obtained from the ORFeome library (internal ID: 10073). The crystal structure of BAIAP2 has previously been solved[28]. We generated the isolated I-BAR domain construct spanning amino acids 1–252:

Other constructs, LOV–RAC1 (ref. 20), f-tractin[29], Lyn–FRB (ref. 30), CFP–FKBP–TIAM1 (ref. 30) and NMHC-II-A (ref. 31) (Addgene no. 11347) were previously described.

Cell transfection. Proteins were transfected with Lipofectamine 2000 (Invitrogen, no. 11668) according to the manufacturer's protocol. Excessive overexpression of full-length and the isolated N-BAR domain of amphiphysin 1 led to aggregation that induced deformations of the plasma membrane. Amphiphysin 1 promoted invaginations that originated at the plasma membrane and occasionally polymerized forming dynamic, tubular structures that protruded into the cytosol. Supporting our notion that N-BAR domain proteins do not deform the plasma membrane at the native concentration, membrane tubulation did not occur at low expression levels. To account for this potential overexpression artefact, all experiments on nanocones were performed 12–24 h post-transfection, when expression was still low, and cells that exhibited visible large protein aggregates were excluded.

Live-cell microscopy. Live-cell dual-colour measurements were performed on a spinning-disc confocal microscope. CFP and YFP were excited using the 442 nm line of a helium cadmium laser (100 mW; Kimmon Electrics) and the 514 nm line of an argon laser (300 mW; Melles Griot), respectively. Images were captured using an EMCCD (electron-multiplying charge-coupled device) camera (QuantEM 512SC), driven by Micromanager which was mounted on the side port of an inverted microscope (model IX-71; Olympus). Co-localization studies were carried out on a custom-made prism-based total internal reflection fluorescence microscope using an EMCCD camera (QuantEM 512SC) driven by Micromanager.

Background subtraction algorithm. For better visualization, images Fig. 2b,c were processed in Matlab using a high-pass filter (http://www.csse.uwa.edu.au/~pk/Research/MatlabFns/FrequencyFilt/highpassfilter.m).

Spatial cross-correlation analysis. Spatial cross-correlation of individual images in Supplementary Figs S1b and S2d–f was assessed using the Matlab function xcorr.

Drugs. The following inhibitors were used: latrunculin A (4 μM; Cal Biochem no. 428026); cytochalasin D (5 μM; Invitrogen no. PHZ1063), ML-7 (20 μM; Santa Cruz Biotechnology no. sc-200553A).

FKBP–TIAM1 assay. 3T3 cells were triple-transfected with Lyn–FRB, CFP–FKBP–TIAM1 and the YFP-tagged N-BAR domain of amphiphysin 1. At 12–24 h post-transfection, individual cells were imaged before and at 10 s intervals after the addition of 100 nM rapamycin (Sigma-Aldrich, no. B0560) with a ×63 objective and an ×1.5 Optovar module.

DOI: 10.1038/ncb2533

LOV–RAC1 assay. HeLa cells were typically co-transfected with CFP–LOV–RAC1 and a YFP-tagged gene of interest, using Lipofectamine 2000 and imaged 12–36 h after transfection. All experiments were performed with constitutively active CFP–LOV–RAC1. Cells with relatively high LOV–RAC1 expression levels were identified (on the basis of CFP fluorescence) and selected for the light-induced translocation studies. As LOV–RAC1 activity is triggered with blue light[20], acquisition of CFP–LOV–RAC1 using a 442 nm laser automatically activated the construct. Identified cells were therefore kept in the dark for 5 min to allow the LOV domain to refold (half-life of LOV–RAC1 for refolding is 43 s; ref. 20) before imaging. Subsequently, YFP followed by a CFP image were acquired and compared with a second image pair obtained 15 s later. For each cell, membrane-localized puncta of N-BAR domain proteins were identified using the find Maxima function in ImageJ. Individual thresholds were manually adjusted for the pre-activation image, and then applied the same way to the post-activated image. The negative ratio of pre/post puncta stimulation in the experiments without LOV–RAC reflects a fraction of the puncta (<5%) falling below the detection level probably owing to a slight photobleaching.

Temporal cross-correlation analysis. Temporal cross-correlation has been previously described[32]. In brief, a mask of the migrating cell was generated for individual frames and each pixel at the boundary was identified, containing information of N-BAR and f-tractin intensity. Individual pixels (at the cell boundary) were tracked over multiple frames, allowing analysis on position and velocity of the lamellipodia. Finally, temporal cross-correlation between the ratio of N-BAR intensity to f-tractin intensity with respect to the localization of the cell boundary for each pixel was analysed.

Statistical analysis. Statistical significance was tested using the two-tailed Student *t*-test. The results from individual experiments are presented as mean values; error bars depict the s.e.m.

26. Shimada, A. *et al*. Curved EFC/F-BAR-domain dimers are joined end to end into a filament for membrane invagination in endocytosis. *Cell* **129,** 761–772 (2007).
27. Henne, W. M. *et al*. Structure and analysis of FCHo2 F-BAR domain: a dimerizing and membrane recruitment module that effects membrane curvature. *Structure* **15,** 839–852 (2007).
28. Millard, T. H. *et al*. Structural basis of filopodia formation induced by the IRSp53/MIM homology domain of human IRSp53. *EMBO J.* **24,** 240–250 (2005).
29. Johnson, H. W. & Schell, M. J. Neuronal IP3 3-kinase is an F-actin-bundling protein: role in dendritic targeting and regulation of spine morphology. *Mol. Biol. Cell* **20,** 5166–5180 (2009).
30. Inoue, T., Heo, W. D., Grimley, J. S., Wandless, T. J. & Meyer, T. An inducible translocation strategy to rapidly activate and inhibit small GTPase signaling pathways. *Nat. Methods* **2,** 415–418 (2005).
31. Wei, Q. & Adelstein, R. S. Conditional expression of a truncated fragment of nonmuscle myosin II-A alters cell shape but not cytokinesis in HeLa cells. *Mol. Biol. Cell* **11,** 3617–3627 (2000).
32. Tsai, F. C. & Meyer, T. Ca(2+) pulses control local cycles of lamellipodia retraction and adhesion along the front of migrating cells. *Curr. Biol.* **22,** 837–842 (2012).

DOI: 10.1038/ncb2533

nature cell biology

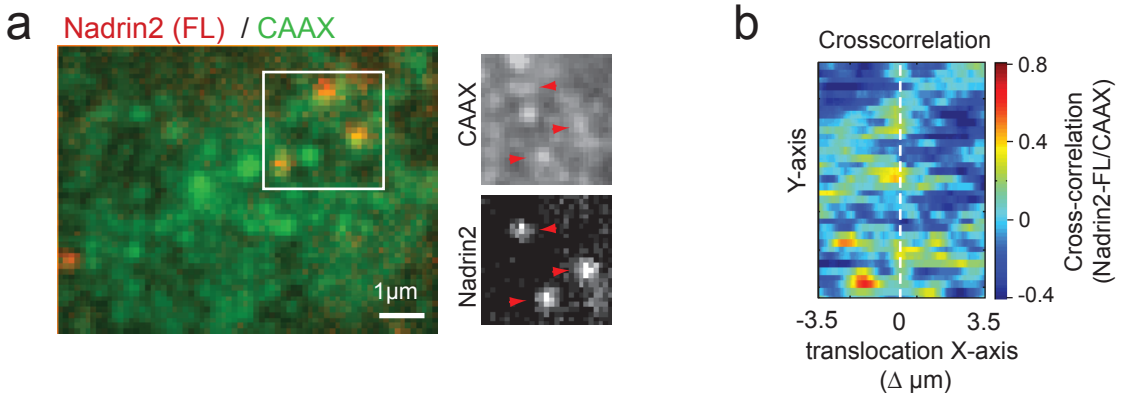

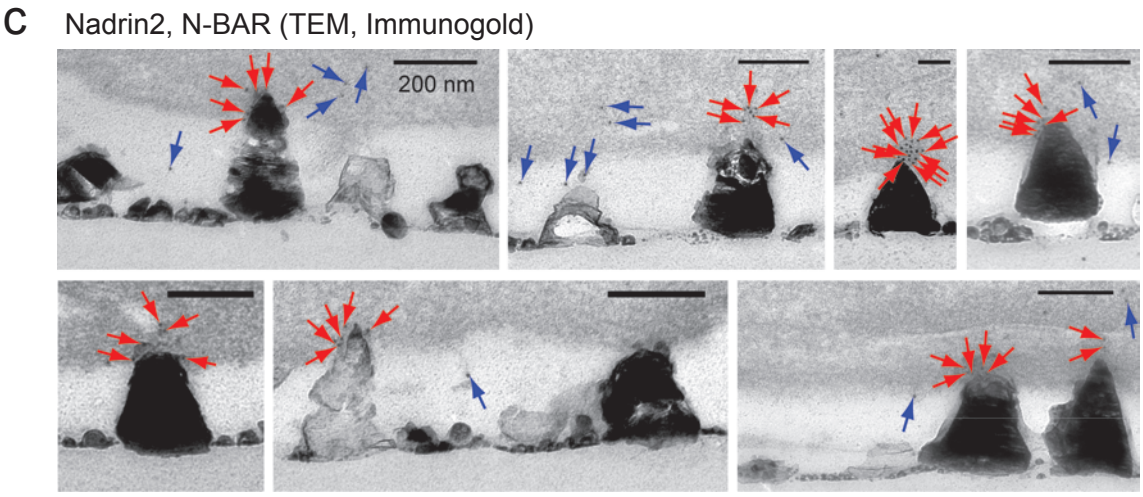

Figure S1 N-BAR domain recruitment to Nanocones is curvature-dependent. **(a)** 3T3 cells cultured on Nanocones were transfected with the full length version of nadrin 2 (red) and the membrane marker CAAX (green). For better visualization, a magnified section (white box) of the individual channels is shown to the right. Note non-uniform fluorescent intensity for the membrane marker, likely reflecting individual or groups of Nanocones that deform the plasma membrane, causing membrane accumulation in the z-direction. Nadrin 2 puncta occurred on top of individual puncta. However, N-BAR domain puncta appeared not on all membrane indentations. **(b)** Correlation analysis for full length nadrin 2 (red) and the membrane marker CAAX (green). Note, no significant drop in correlation is evident for nadrin 2 vs. CAAX upon lateral shift. **(c)** Transmitted electron micrographs show accumulation of immunogold particles directed against the isolated N-BAR domain of nadrin 2 to inward curved plasma membranes formed by Nanocones (red arrows). 3T3 cells were transfected with a fluorescently tagged N-BAR domain of nadrin 2 and plated on Nanocones. Fluorescently tagged N-BAR domain of nadrin 2 is detected with polyclonal anti-GFP antibody and visualized with gold-conjugated secondary antibodies. Note the increased density of gold particles on inward curved membranes on top of Nanocones (red arrows) compared to the cytosolic background (blue arrows), indicative of a curvature-sensing recruitment of the N-BAR domain to such sites. Scale bars; (a), 1 µm; (c), 200nm.

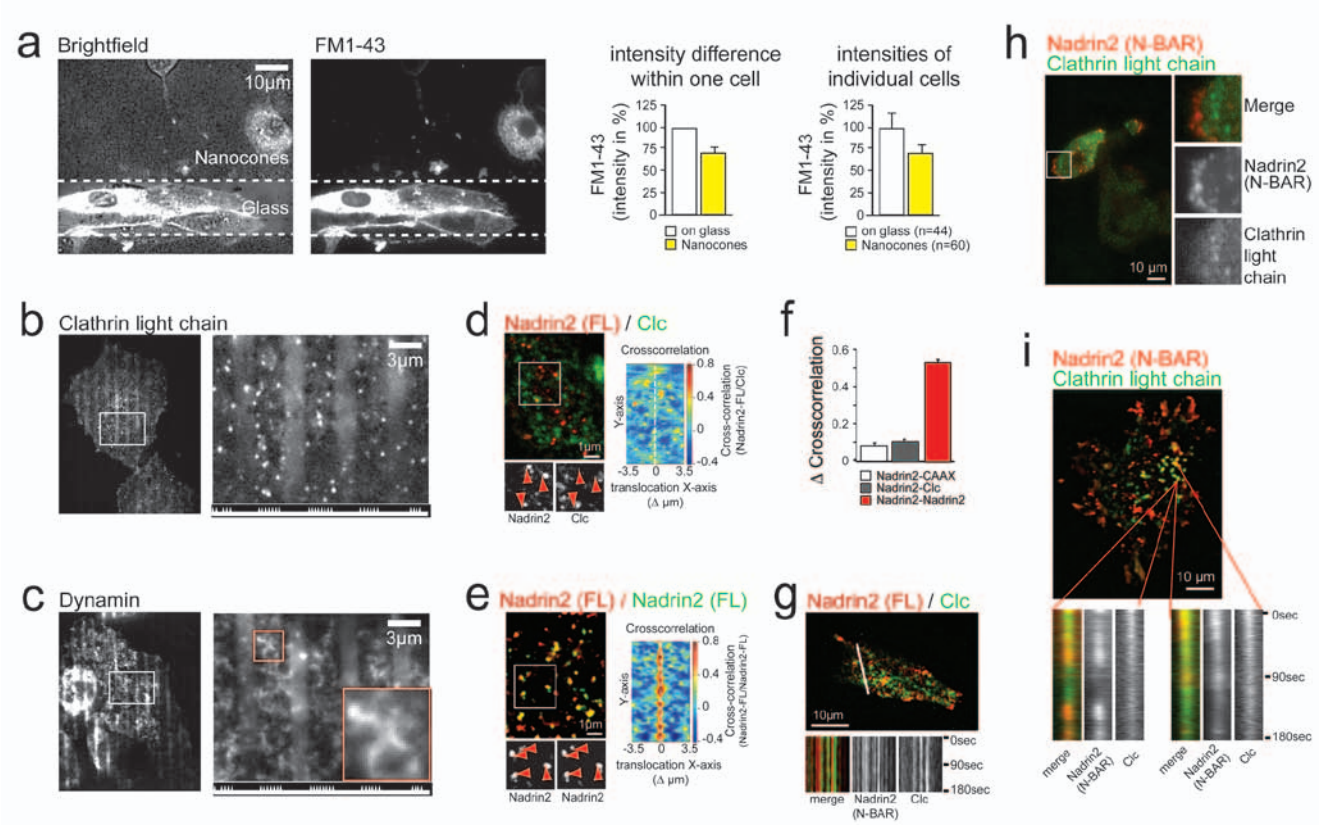

Figure S2 N-BAR domain proteins recruit to Nanocone-triggered inward curved sections of the PM independently of clathrin-dependent endocytotic events. **(a)** Nanocones do not increase the average endocytosis rate. FM1-43 uptake assay shows that the average fluorescent intensity within the same cell (left graph) was reduced 28+/-8% by the Nanocones. The average fluorescent intensity of cells grown on Nanocones (right graph) was 27+/-5% less than for cells grown on glass. Nanocone-dependent change in intensity within a single cell was measured for 20 cells (left graph). Average intensities were measured for 44 cells on glass and 60 cells on Nanocones (right graph). Error bars represent s.e.m. of the mean value. **(b, c)** Endocytotic proteins are enriched over Nanocones. 3T3 cells over-expressing fluorescently tagged clathrin light chain (b) or dynamin (c) were grown on 3µm wide stripes of Nanocones. Both proteins were enriched over stripes of Nanocones. For better visualization, a magnified section is shown to the right (white box). Note, that dynamin-aggregates on Nanocones formed tubular structures (red box). **(d)** Correlation analysis for full length nadrin 2 (red) with clathrin light chain (Clc, green) shows low colocalization. Single channels for the inset (white) are shown below. **(e)** Control correlation analysis for CFP-tagged full length nadrin 2 (red) with YFP-tagged full length nadrin 2 (green). Magnification of single channels are shown below. **(f)** Panel depicting difference in correlation-score for the two channels before and after a lateral shift by 10 pixel (=1.6µm). Error bars represent s.e.m. for the 125 individual rows (y-axis) of the heatmap shown in panels (d) and (e). Note the significant drop in correlation for nadrin 2 vs. nadrin 2 (red) but not for nadrin 2 vs. membrane (white) and nadrin 2 vs. clathrin light chain (gray). **(g)** N-BAR domain and clathrin light chain puncta on Nanocones remain separate over time. 3T3 cell plated on Nanocones were transfected with fluorescently tagged N-BAR domain of nadrin 2 (red) and clathrin light chain (green) and imaged every 5 second for 3 minutes. Kymograph depicting traces of individual puncta are shown below. **(h)** In the absence of Nanocones, the N-BAR domain of nadrin 2 does not colocalize with markers for clathrin-dependent endocytosis at the leading edge of migrating 3T3 cells. Cells were co-transfected with the N-BAR domain of nadrin 2 (red) and clathrin light chain (green), a marker for clathrin-dependent endocytosis and imaged 24h later on a TIRF microscope. The N-BAR domain did not colocalize with endocytic sites at the leading edge. **(i)** In the absence of Nanocones, the N-BAR domain of nadrin 2 is transiently recruited to endocytic sites at the center of the cell. Cells were imaged on a TIRF for 3 minutes. Kymograph shows pulsatile appearance of the isolated N-BAR domain of nadrin 2 (red) to these sites, indicating transient formation of curved plasma membrane sites by clathrin light chain (green). Scale bars (a, g, h, i), 10 µm; (b, c), 3 µm; (d, e), 1 µm.

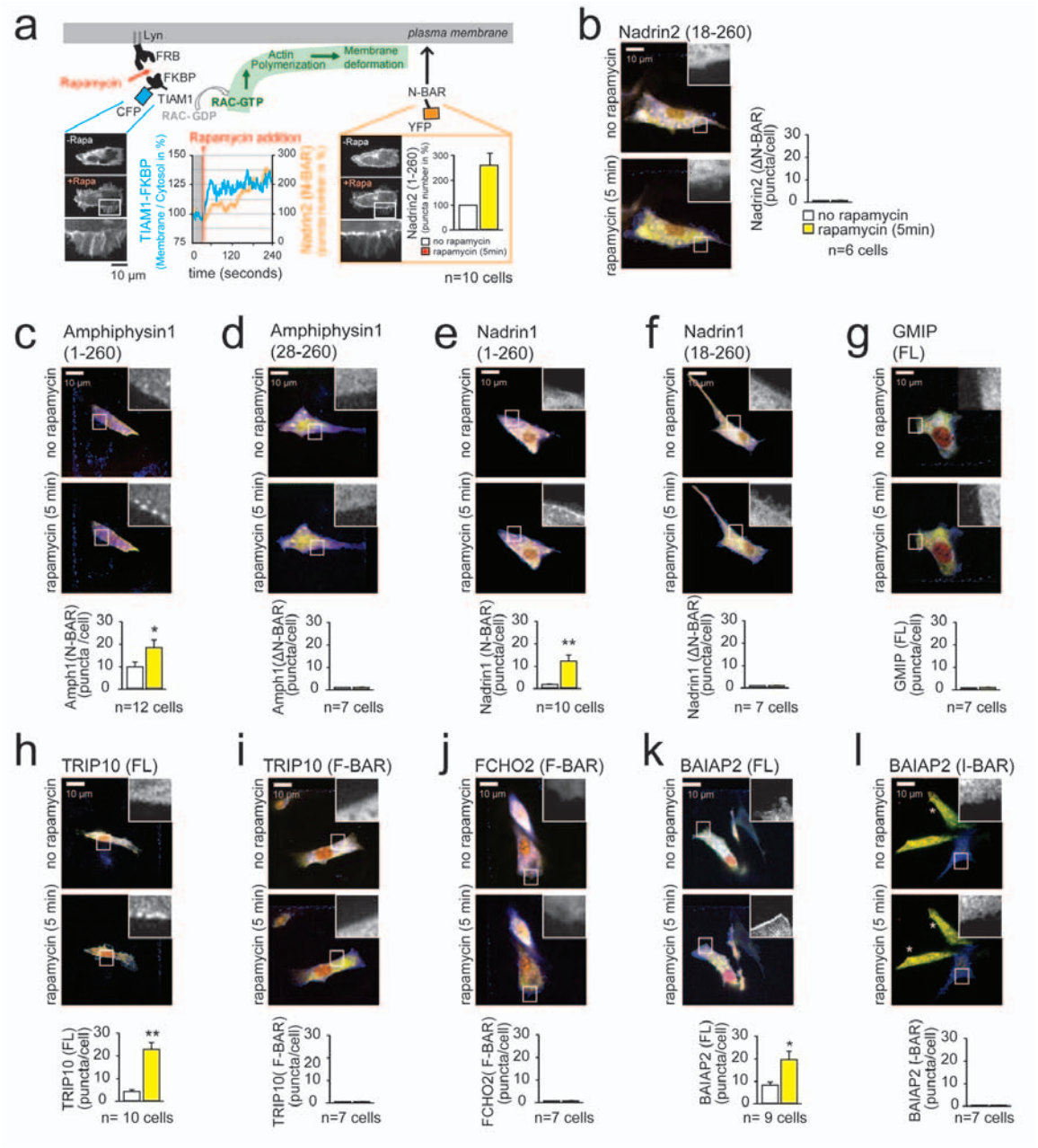

Figure S3 Rapamycin-induced actin polymerization triggered BAR domain puncta formation in 3T3 cells. **(a)** 3T3 cells were co-transfected with a membrane-anchored FRB, as well as with fluorescently and FKBP-tagged Rho-GEF TIAM1 and the N-BAR domain of nadrin 2. Addition of rapamycin triggered hetero-dimerization of FRB and FKBP triggering rapid translocation of FKBP-TIAM1 to the PM (blue, left panels). With a delay, this triggered formation of RAC-GTP, causing excessive lamellipodia formation and translocation of the N-BAR domain of nadrin 2 (orange, right graph). **(b)** No translocation is observed when the amphipatic helix, encoded by the first 18 amino acids of the N-BAR domain of nadrin 2 is deleted. **(c)** Addition of rapamycin-induced translocation of the isolated N-BAR domain of amphiphysin 1. **(d)** No translocation is observed when the amphipatic helix of amphiphysin 1, encoded by the first 28 amino acids is deleted. **(e)** Addition of rapamycin-induced translocation of the isolated N-BAR domain of nadrin1. **(f)** No translocation is observed when the amphipatic helix, encoded by the first 18 amino acids of nadrin1 is deleted. **(g)** Addition of rapamycin does not induce translocation of the BAR domain protein GMIP. **(h)** Addition of rapamycin-induced translocation of the F-BAR domain protein TRIP10. **(i)** No translocation is observed when the isolated F-BAR domain of TRIP10, encoded by the first 298 amino acids is expressed separately. **(j)** As for TRIP10, no translocation is observed for the isolated F-BAR domain of FCHO2 (AA1-274). **(k)** Addition of rapamycin-induced translocation of full length BAIAP2. **(l)** No translocation is observed when the isolated I-BAR domain of BAIAP2, encoded by the amino acids 1-252 is expressed. Scale bars, 10µm. Error bars represent s.e.m. of the mean value. $^{**}P < 0.01$.

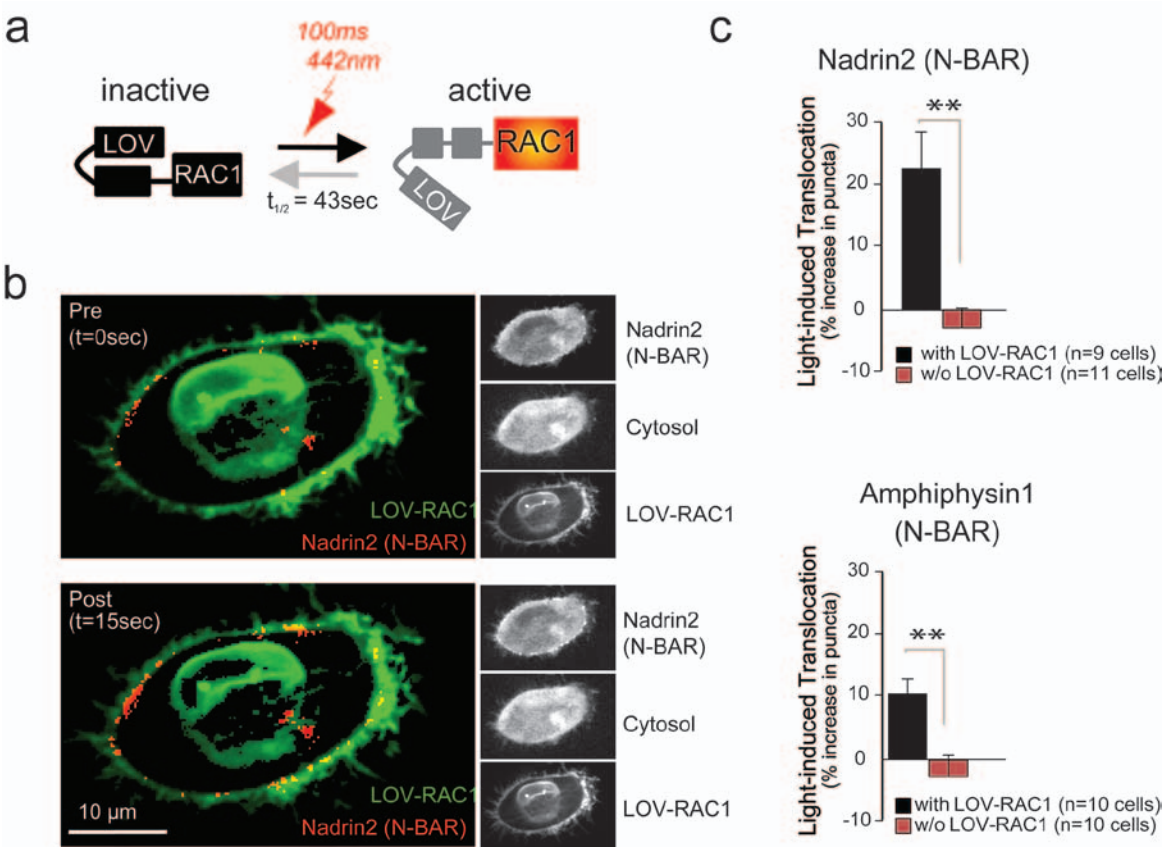

Figure S4 Induction of actin-dynamics caused recruitment of N-BAR domain proteins to the plasma membrane. **(a)** Scheme of the LOV-RAC1 activation mechanism. Exposure of blue light induces a conformational change of the LOV domain which exposes the constitutive active form of RAC1. Activity of RAC1 ends when the LOV domain returns to its native state. **(b)** The LOV-RAC1 (green) was activated with a 100ms pulse of 442nm light. Within 15 seconds the isolated N-BAR domain of nadrin 2 (red) was recruited in punctate to the plasma membrane. For better illustration, the images were background-subtracted. As a reference, original images depicting the N-BAR domain or nadrin 2 (top), a cytosolic reference (middle) and LOV-RAC1 (bottom) are shown next to the images. Note that LOV-RAC1 strongly enriched at the nuclear membrane while no N-BAR domain puncta located to this structures. At the plasma membrane, LOV-RAC1 was uniformly distributed while the N-BAR domain of nadrin 2 appeared in puncta facing the cytosol. Together, these data suggest that translocation of the N-BAR domain is not due to direct interaction with the RAC1 upon light-activation. **(c)** Analysis of the observed increase in puncta density is shown to the right for the isolated N-BAR domain of nadrin 2 (top) and amphiphysin 1 (bottom). Error bars represent s.e.m. of the mean value. Scale bar, 10µm. ** $P < 0.01$.

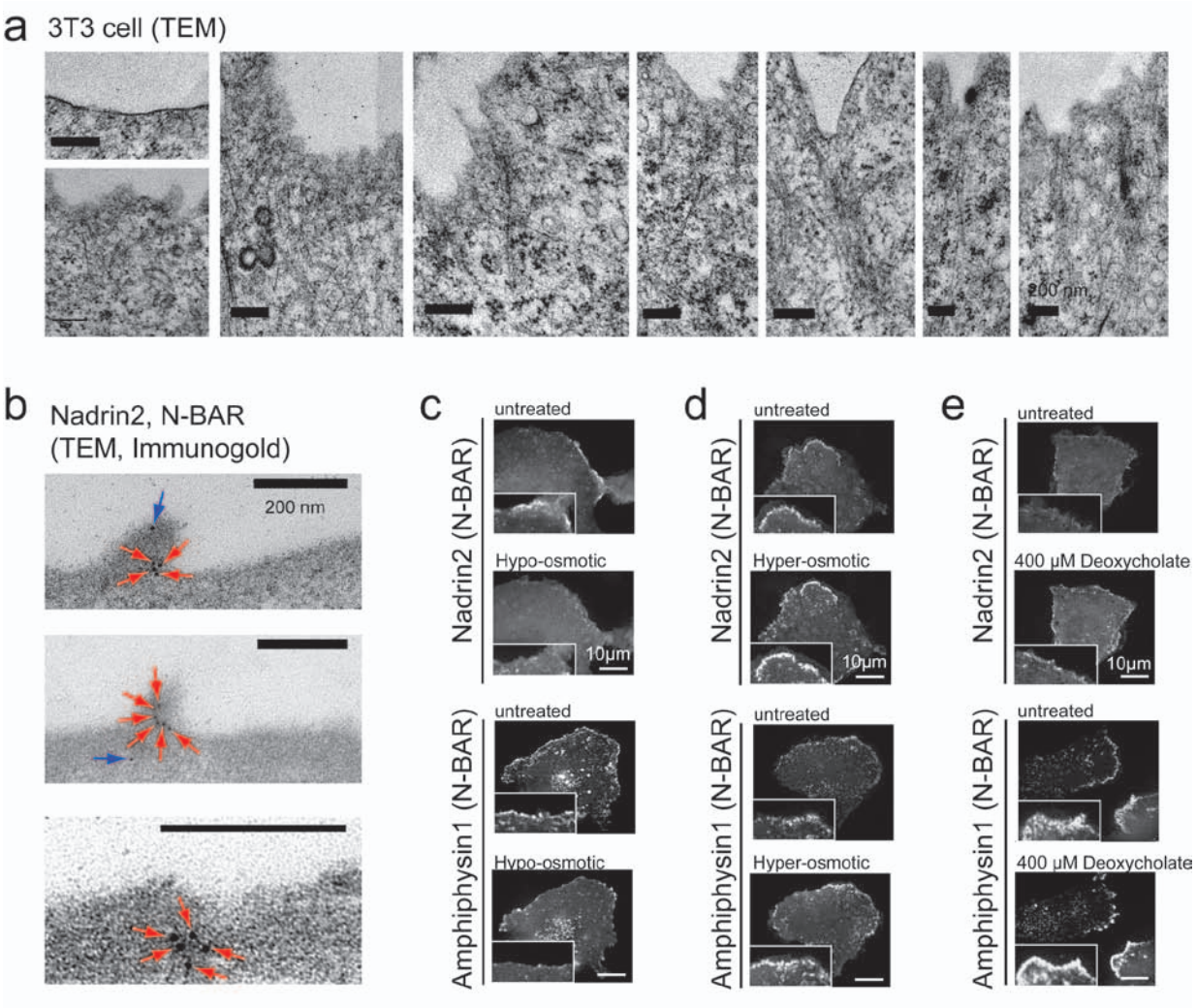

Figure S5. Actin cables pulling at the plasma membrane recruit curvature-sensing N-BAR domain proteins. **(a)** Transmitted electron micrographs of 3T3 cells cut parallel to the surface and contrast enhanced with osmium tetroxide. One sample with no actin filaments visible (top, left) and seven samples with actin filaments extending to the PM are shown. Note that actin filaments are oriented perpendicular to the plasma membrane ending close to deformed section of the plasma membrane. **(b)** Fluorescently tagged N-BAR domain of nadrin 2 is detected with polyclonal anti-GFP antibody and visualized with gold-conjugated secondary antibodies. Note the high density of gold particles associate with curved regions (red arrows) of the plasma membrane compared to the low cytosolic background (blue arrows). **(c)** Membrane tension controls N-BAR domain puncta formation. Hypo-osmotic shock dissolved N-BAR domain puncta in COS cells. Cells were transfected with YFP tagged N-BAR domain of nadrin 2 (top) and amphiphysin 1 (bottom). After replacement of regular medium (DMEM+10%PBS; 310+/-10 mOsm/kg) with pre-warmed hypo-osmotic medium (1:6 dilution of medium:ddH2O; 50 mOsm/kg) the N-BAR domain puncta disappeared within 200 seconds. **(d)** Hyper-osmotic shock increased N-BAR domain puncta density. Addition of hyper-osmotic medium (regular medium supplemented with 1% 10x PBS; 340+/-10 mOsm/kg) triggered an increase in N-BAR domain puncta number for nadrin 2 (top) and amphiphysin 1 (bottom) within 100 seconds. **(e)** . Membrane relaxation caused rapid increase in N-BAR domain puncta number. N-BAR domain puncta number of nadrin 2 and amphiphysin 1 increased within 60 seconds after addition of 400 μM Deoxycholate. Scale bars, (a, b), 200nm; (c-e), 10μm.